Journal of Power Sources 311 (2016) 81–90

Contents lists available at ScienceDirect

Journal of Power Sources

journal homepage: www.elsevier.com/locate/jpowsour

A comparative investigation of metal-support interactions on the catalytic activity of Pt nanoparticles for ethanol oxidation in alkaline medium

Denis R.M. Godoi [a], Hebe M. Villullas [a, *], Fu-Chun Zhu [b], Yan-Xia Jiang [b], Shi-Gang Sun [b], Junsong Guo [c], Lili Sun [c], Rongrong Chen [c]

[a] Instituto de Química, Universidade Estadual Paulista – UNESP, 14800 Araraquara, SP, Brazil
[b] State Key Laboratory of Physical Chemistry of Solid Surfaces, Department of Chemistry, College of Chemistry and Chemical Engineering, School of Energy Research, Xiamen University, Xiamen, 361005, China
[c] Richard G. Lugar Center for Renewable Energy, Indiana University–Purdue University, Indianapolis, IN, 46202, United States

HIGHLIGHTS

- Pt nanoparticles on hybrid C-MOx supports have different EOR activities.
- Metal-support interactions affect the Pt 5d vacancy.
- EOR activity in alkaline solution follows the Pt 5d band vacancy.
- Acetate is the main oxidation product but CO_2 selectivity changes with support.
- Fuel cell performances are in agreement with electrochemical and FTIR results.

ARTICLE INFO

Article history:
Received 14 October 2015
Received in revised form
31 January 2016
Accepted 4 February 2016
Available online 17 February 2016

Keywords:
Ethanol oxidation
Metal-support interactions
FTIR spectroscopy
Alkaline fuel cell

ABSTRACT

The effects of interactions of Pt nanoparticles with hybrid supports on reactivity towards ethanol oxidation in alkaline solution are investigated. Studies involve catalysts with identical Pt nanoparticles on six hybrid supports containing carbon powder and transition metal oxides (TiO_2, ZrO_2, SnO_2, CeO_2, MoO_3 and WO_3). *In situ* X-ray absorption spectroscopy (XAS) results evidence that metal-support interactions produce changes in the Pt 5d band vacancy, which appears to determine the catalytic activity. The highest and lowest activities are observed for Pt nanoparticles on hybrid supports containing TiO_2 and CeO_2, respectively. Further studies are presented for these two catalysts. *In situ* FTIR reflection spectroscopy measurements, taken using both multi-stepped FTIR spectroscopy (MS-FTIR) and single potential alteration FTIR spectroscopy (SPA-FTIR), evidence that the main product of ethanol oxidation is acetate, although signals attributed to carbonate and CO_2 indicate some differences in CO_2 production. Fuel cell performances of these catalysts, tested in a 4.5 cm^2 single cell at different temperatures (40–90 °C) show good agreement with data obtained by electrochemical techniques. Results of this comprehensive study point out the possibility of compensating a reduction of noble metal load with an increase in activity promoted by interactions between metallic nanoparticles and a support.

1. Introduction

The growing awareness regarding the necessity of sustainable and environment-friendly energy production resulted in a continuously rising interest in the development of technologies based on renewable sources. This scenario brought about an increase in the research directed to different aspects of fuel cells (FCs) development, mainly due to the high theoretical efficiency of these devices [1]. Moreover, while the electrochemical conversion of chemical energy into electricity is appropriate for stationary power generation, it is also uniquely suitable for application in vehicles and portables.

Various fuels can be used to feed FCs, but ethanol is particularly

* Corresponding author.
E-mail address: mercedes@iq.unesp.br (H.M. Villullas).

http://dx.doi.org/10.1016/j.jpowsour.2016.02.011
0378-7753/

attractive because it can be produced from biomass, such as sugarcane, corn and other grains, and agricultural waste [2]. As result, the research dedicated to Direct Ethanol Fuel Cells (DEFC) development grew significantly over the last two decades [3,4] and a number of investigations of EOR electrocatalysts were carried out [5–9]. The kinetics and mechanism of the EOR in acid solutions has been studied on Pt model surfaces [10,11] as well as on Pt supported nanoparticles [12]. Despite the progress already made, more efficient catalysts for EOR are still needed to improve DEFCs performances. The C–C bond breaking needed to oxidize the ethanol molecule to CO_2 has remained a challenge, and many studies have demonstrated that the main products of the EOR are acetaldehyde and acetic acid [13–17].

The most successful approach in the search for more effective catalysts for the oxidation of alcohols, such as methanol and ethanol, involves alloying Pt with transition metals [8,18]. On the other hand, the effects of combining Pt particles with oxides acting as co-catalysts or supports were also investigated. While some of those studies of Pt catalysts containing transition metal oxides, such as WO_3 [19,20], CeO_2 [21–24], ZrO_2 [25], SnOx [26] and SnO_2 [27], and RuO_2 [28,29] were published several years ago, the relevance of transition metal oxides for the electrocatalysis of fuel cell reactions was pointed out again in recent literature reviews [30,31]. However, as most efforts in the area of low temperature FCs were directed for many years to those devices using a proton exchange membrane (PEM) as electrolyte, the vast majority of EOR studies were carried out in acid environments [30,31].

The development of anion-exchange membranes [32,33] made the possibility of producing energy using alkaline DEFCs quite attractive [34]. This renewed interest in alkaline environments triggered a significant increase in the number of studies in alkaline media in which more metals are active for the oxidation of alcohols and the reaction kinetics is faster [35]. At the same time, some studies carried out in alkaline solutions revealed that trends of catalytic activity were different from those observed in acid environments [36].

In a general manner, most data on the effects of transition metal oxides were taken in acid solutions. On the other hand, they are difficult to compare as studies involved different conditions and because the catalysts usually had different compositions and Pt nanoparticles of different sizes. Several explanations were given for activity changes promoted by the transition metal oxide, such as better dispersion of Pt particles on the support, changes in the Pt 5d band vacancies and contribution of OH groups present at the oxide surface to the bifunctional mechanism in the case of alcohols oxidation. Altogether, literature data are still insufficient to draw general conclusions for any given reaction.

To the best of our knowledge, systematic studies of the effects of metal-support interactions on electronic properties and their impact on EOR reaction rate and mechanism were never published. In this work, a comprehensive study of the effects of the interactions between Pt nanoparticles and hybrid supports C-MOx (MOx = TiO_2, ZrO_2, SnO_2, CeO_2, MoO_3 and WO_3) on the activity for the EOR in alkaline solutions is presented, as well as data from spectroscopic studies of product distribution and results of fuel cell testing for selected catalysts.

2. Experimental

2.1. Catalysts preparation and characterization

A colloidal dispersion of Pt nanoparticles was prepared by a modified polyol method [37]. The synthesis was carried out in dioctyl ether in the presence of a long-chain diol (1,2 hexadecanediol) that acted as reducer and under Ar atmosphere. Oleylamine and oleic acid were used as capping agents. Briefly, 0.0812 g of the metal precursor (Platinum(II) acetylacetonate, Sigma-Aldrich, 97%) were dissolved in 15 mL of dioctyl ether (Sigma-Aldrich, 99%) together with 160.8 mg of 1,2-hexadecanediol (Sigma-Aldrich, technical grade, 90%). The mixture was first heated to 110 °C and, after addition of 270 μL of oleic acid (Sigma-Aldrich, technical grade, 90%) and 390 μL of oleylamine (Sigma-Aldrich, technical grade, 70%), the temperature was raised until reflux (about 298 °C). After keeping the system under reflux for 30 min to complete the reaction, the system was allowed to cool to room temperature. After that, the Pt nanoparticles were separated and thoroughly cleaned as described elsewhere [38].

The hybrid supports were prepared by mixing suspensions of carbon powder (Vulcan XC-72, Cabot Corp.) with commercial nanopowders of transition metal oxides (MOx) suspended in isopropanol. All hybrid supports were prepared containing 80 wt% carbon powder and 20 wt% MOx. Oxide particle sizes were <100 nm for ZrO_2, SnO_2, MoO_3 and WO_3 and <50 nm for CeO_2 and TiO_2. The Vulcan XC-72 carbon powder was heat-treated in Ar atmosphere before use [39].

In order to warrant that all catalysts had Pt particles with identical properties, fractions of the same colloidal suspension of Pt nanoparticles were used to prepare the catalysts. In this way, the only difference between catalysts was the transition metal oxide in the hybrid support. For the supporting step, proper amounts of Pt nanoparticles dispersed in hexane and support dispersed in isopropyl alcohol were mixed and then constantly stirred for 12 h. The resulting material was filtered, exhaustively washed with ethanol, acetone, and water, and dried. All catalysts had 20 wt% Pt loading. A Pt/C catalyst was also prepared with one portion of the colloidal suspension of the Pt nanoparticles and used as reference material.

Transmission electron microscopy (TEM) studies were carried out using a FEI TECNAI G^2 F20 HRTEM instrument, which also allowed energy dispersive X-ray analysis (EDX).

X-ray photoelectron spectroscopy (XPS) experiments were carried out at the Brazilian Nanotechnology National Laboratory (LNNano) with a K-ALPHA surface analysis spectrometer (Thermo Scientific, Inc.). Spectra were collected using Al Kα radiation (1486.6 eV) in constant energy analyzer mode with energy pass of 30 eV and energy steps of 0.1 eV.

The electronic properties of all catalysts were studied by *in situ* X-ray absorption spectroscopy (XAS) experiments performed around the Pt L_3 edge (11564.25 eV) at the XAFS1 beamline of the Brazilian Synchrotron Light Laboratory (LNLS). These measurements were done in a spectroelectrochemical cell with similar configuration to that reported elsewhere [40], using a Pt mesh as counter electrode and a reversible hydrogen reference electrode. The working electrode was a pellet obtained by pressing a mixture of 30 mg of catalyst powder and 400 μL of Nafion® solution (Aldrich, 5 wt% in a mixture of alcohols and water) on a carbon cloth. All working electrodes for these experiments had a constant Pt loading of 6 mg cm^{-2}. Measurements were carried out in 0.1 M KOH solutions and at constant applied potential.

2.2. Electrochemical measurements

All electrochemical measurements were performed in a conventional electrochemical cell, with a platinized Pt wire counter electrode placed in a separate compartment and a reversible hydrogen reference electrode. The catalysts were used as ultra-thin layers deposited on a glassy carbon disk electrode (0.196 cm^2) previously polished down to 0.3 μm alumina. The Pt loading was 28 μg cm^{-2}. The catalyst ink was prepared with 2.9 mg of catalyst dispersed in isopropyl alcohol and 15 μL of Nafion® solution. The general electrochemical behavior was characterized by cyclic

voltammetry (CV) in 0.1 M KOH solution, and the electrocatalytic activity for the EOR was evaluated in Ar-saturated 0.5 M ethanol in 0.1 M KOH solutions through CV and chronoamperometry (CA) experiments. CO stripping experiments were carried out in 0.1 M KOH solutions. CO was admitted to the cell and adsorbed at 0.15 V vs. RHE for 20 min. After removing the excess CO by bubbling Ar through the solution during 20 min, the adsorbed CO was oxidized at a scan rate of 5 mV s^{-1}. All experiments were performed at 25 °C.

2.3. Fuel cell testing

All experiments were performed in a single cell with an active area of 4.5 cm^2. The membrane electrode assemblies (MEA) were comprised of a catalyst coated membrane (CCM), a Ni foam (Hohsen Corp.) as the anode backing layer and a TGP-H-090 carbon paper (Toray) as the cathode backing layer. The anode catalyst ink was prepared by mixing 16 mg of catalyst with Nafion solution. The cathode catalyst ink was prepared by ultrasonicating 8 mg of nanorod MnO_2 catalyst, 8 mg of active carbon (BP2000, Cabot Corp.), and the A4 ionomer (Tokuyama Co.). The catalyst:ionomer weight ratio was 80:20 for the anode and for the cathode. After homogenizing by sonication, the inks were airbrushed onto a 6.25 cm^2 Tokuyama A201 membrane (Tokuyama Co.) to form a CCM. The MEA was sandwiched between two graphite bipolar plates. The fuel cell tests were conducted on a Scribner Associates Model 850e test station following the test protocols developed by Chen's group [41]. The liquid fuel (ethanol in KOH solution) was pumped to the anode at a rate of 2 mL min^{-1}. Oxygen gas (Praxair Inc.) humidified at 30 °C was fed to the cathode at 300 sccm. Measurements were carried out at different fuel cell temperatures (40–90 °C), which were maintained constant with a tolerance of 0.2 °C. The polarization curves were obtained by measuring the cell voltage at different currents after reaching steady state.

2.4. In situ FTIR studies

Electrochemical *in situ* FTIR reflection spectroscopy was carried out on a Nexus 8700 spectrometer (Nicolet) equipped with a liquid-nitrogen-cooled MCT-A detector. The experiments were performed in a three-electrode IR cell where the thin layer of electrolyte was formed by pressing the working electrode against the CaF_2 window. For these experiments, a platinized Pt foil was used as counter electrode and a saturated calomel electrode (SCE) as reference electrode. The catalyst suspension was prepared with 1.0 mg of catalyst and 1.0 mL of isopropanol. The catalyst layer was prepared depositing 5 μL of the suspension on a 5 mm diameter glassy carbon disk embedded in a Teflon holder, which was allowed to dry in air before depositing a volume of 5 μL of Nafion solution (5 wt%). After drying in air, the electrode was washed with pure water before being placed into a conventional three-compartment cell containing 0.1 M NaOH solution, where it was electrochemically cleaned by potential cycling between −0.94 and 0.01 V vs SCE. Once an unchanging CV curve was obtained, the electrode was transferred to 0.5 M ethanol in 0.1 M NaOH solution, and *in situ* FTIR measurements were performed. Spectra were collected using both multi-stepped FTIR spectroscopy (MS-FTIR) [42] and single potential alteration FTIR spectroscopy (SPA-FTIR) [43]. The resulting spectra are reported as the relative change in reflectivity ($\Delta R/R$), which is calculated as

$$\frac{\Delta R}{R} = \frac{(R(E_S) - R(E_R)}{R(E_R)} \quad (1)$$

where $R(E_S)$ and $R(E_R)$ are the single-beam spectra collected at sample potential E_S and reference potential E_R, respectively.

3. Results and discussion

3.1. Catalysts morphology and electronic properties

Figs. 1a and 1b show a typical TEM image of carbon-supported Pt nanoparticles and the corresponding histogram of particle size distribution. The average particle diameter was found to be 3.5 ± 0.5 nm. It is possible to observe that Pt nanoparticles are well dispersed on the support and that the size distribution is narrow. Bright field and dark field TEM images of Pt nanoparticles on C–CeO_2 and C–TiO_2 hybrid support are shown in Fig. 1c–f, which clearly evidence the presence of oxide nanoparticles as well as Pt nanoparticles on them. EDX analysis confirmed the presence of Pt on top of oxide particles, as exemplified in Supplementary Fig. 1 for the Pt/C–CeO_2 catalyst.

High-resolution XPS spectra of the Pt 4f signal were basically equal for Pt particles on the different hybrid supports. The Pt 4f spectra show similar shapes and width and no shift in peak position was observed, as illustrated in Fig. 2a were, for the sake of clarity, only spectra for three materials are compared. The fact that the Pt 4f signals are essentially identical provide unambiguous evidence that, for the catalysts studied here, metal-support interactions are not strong enough to significantly change the Pt 4f binding energies and that different hybrid support do not have a significant influence on the oxidation state of Pt. A representative high-resolution XPS spectrum of the Pt 4f signal, which after background subtraction (Shirley) was deconvolved in three doublets corresponding to the spin-orbit splitting of the Pt $4f_{7/2}$ and Pt $4f_{5/2}$ components of the different Pt oxidation states, is depicted in Fig. 2b. The line with major intensity is centered at around 71.4 eV and it can be assigned to Pt in the zero-valence metallic state [44]. The slight shift toward higher binding energy with respect to 71.2 eV can be attributed to the small size of Pt nanoparticles [45]. The binding energies of the Pt $4f_{7/2}$ components centered at about 72.3 eV and 74.6 eV can be attributed to Pt(II) and Pt(IV) species [44]. The atomic percentage for each signal was found to be 60.4, 27.5 and 12.1, respectively. XPS high-resolution spectra were also taken for the second transition metal signal (Ti 2p, Zr 3d, Sn 3d, Ce 3d, Mo 3d and W 4f) and allow verifying its incorporation into the hybrid support.

The CV curves recorded in deoxygenated 0.1 M KOH solution at 50 mV s^{-1} and 900 rpm rotation for the Pt catalysts on different carbon-MOx hybrid supports and for the Pt/C reference material are shown in Fig. 3. As expected, CV curves are almost identical, showing only very slight differences due to the contribution of the different MOx components of the supports to double layer charging, and evidencing that all catalysts have nearly the same Pt active area (1.7 cm^2, which is equivalent to *c.a.* 300 $cm^2\ mg_{Pt}^{-1}$). The electrocatalytic activity towards the EOR was initially evaluated performing CV and CA experiments in 0.5 M ethanol in 0.1 M KOH solutions. Results depicted in Figs. 4a and 4b show that the EOR current measured is affected by the support at the time that different oxides in the C-MOx hybrid supports produced different effects. When the ethanol oxidation currents measured for Pt supported on C-MOx hybrids and on Pt/C are compared, it is clear that lower currents were observed for Pt on supports containing CeO_2, WO_3 or ZrO_2. Ethanol oxidation currents were similar for Pt on C–SnO_2 and Pt/C, while a significant current increase is observed for C–TiO_2 and C–MoO_3 supports. For the various transition metal oxides in the hybrid supports studied in this work, the ethanol oxidation current increases in the sequence $CeO_2 < WO_3 < ZrO_2 < C \approx SnO_2 < MoO_3 < TiO_2$.

The interactions of noble metal particles with oxide supports were first revealed in the 70s by Tauster et al. [46], that observed drastic changes in H_2 and CO sorption on noble metals on TiO_2 that were reduced in H_2 at 500 °C, and called them “strong metal

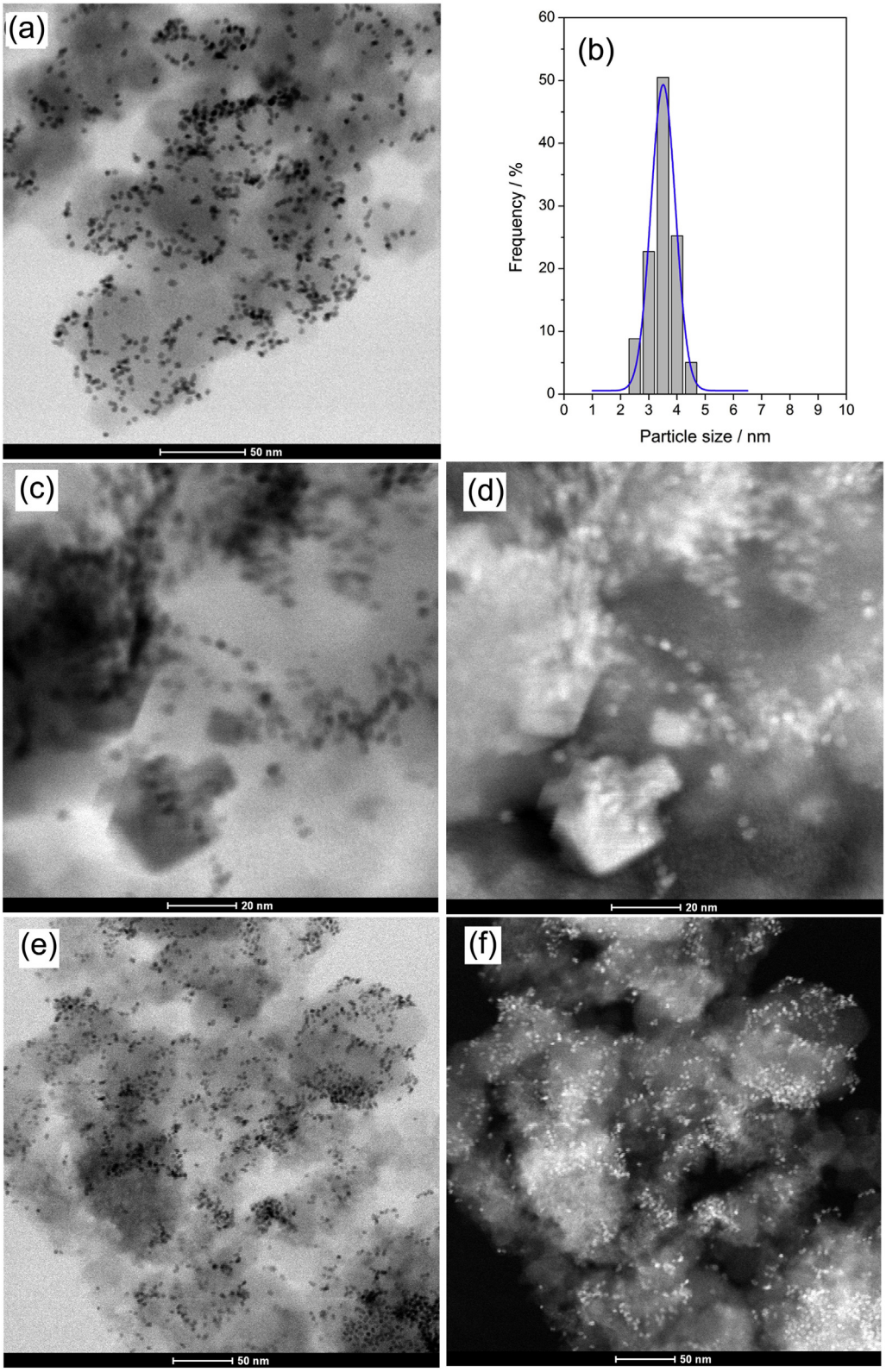

Fig. 1. (a) TEM images of carbon-supported Pt nanoparticles; (b) histogram of particle size distribution; (c) bright field and (d) dark field TEM images of Pt nanoparticles supported on C–CeO_2 hybrid; (e) bright field and (f) dark field TEM images of Pt nanoparticles supported on C–TiO_2 hybrid.

support interactions" (SMSI). The authors considered likely that SMSI would be due to formation of bonds between the noble metal and titanium cations or atoms (overlapping of the occupied d orbitals of the noble metal cation with the vacant d orbitals of Ti^{4+} or formation of an intermetallic compound, respectively). A significant amount of research was soon devoted to SMSI [47–50] and

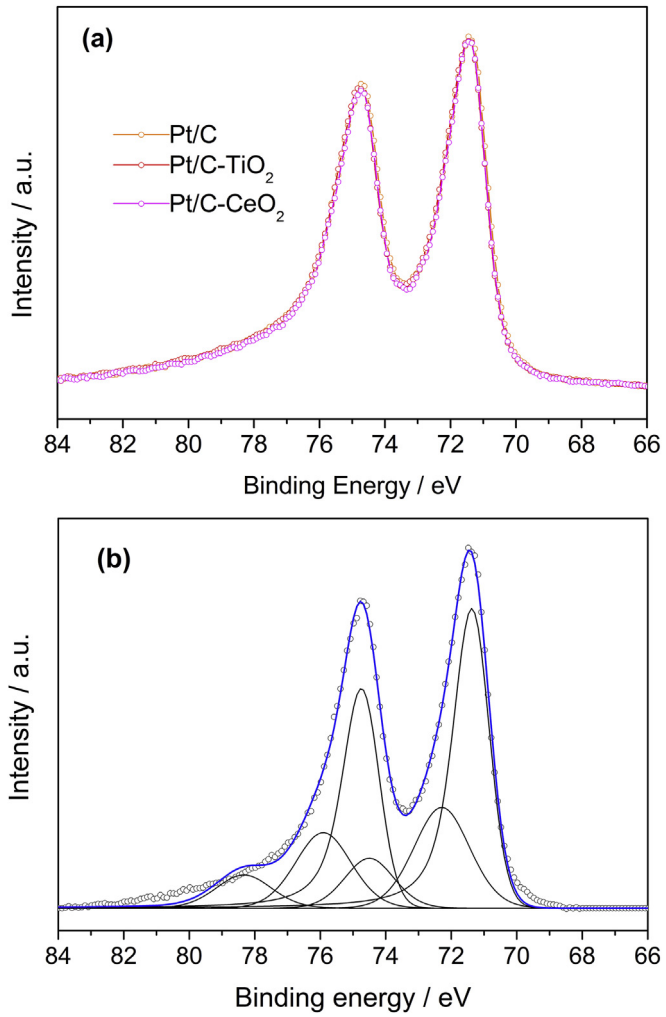

Fig. 2. (a) Comparison of Pt 4f high-resolution XPS data for Pt/C–TiO_2, Pt/C–CeO_2 and Pt/C catalysts. Spectra shown were intensity-normalized after background subtraction (Shirley). (b) Pt 4f high-resolution XPS for Pt/C and deconvolution into three doublets corresponding to the spin-orbit splitting of the Pt $4f_{7/2}$ and Pt $4f_{5/2}$ components of the different oxidation states.

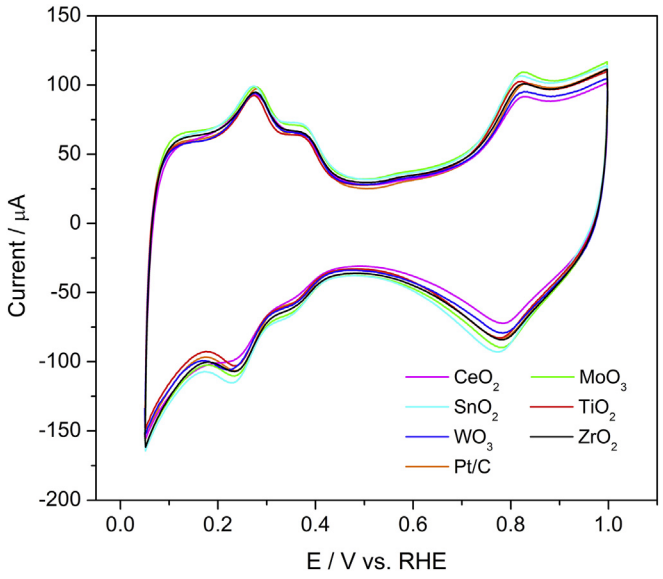

Fig. 3. CV curves recorded in Ar-saturated 0.1 M KOH solution at 50 mV s^{-1} and 900 rpm rotation for the Pt catalysts on different C-MOx hybrid supports. The curve for the carbon-supported catalyst is included for comparison.

other likely interpretations for the effects of metal-support interactions emerged, such a correlation with the reducibility of the saturated transition metal oxides (saturated means, in this case, cations having zero d-orbital occupancy before H_2 treatment) [50] and interactions involving oxygen vacancies in the oxides [49]. Several studies of the effects of composite supports in electrocatalysis were also published, many on oxygen reduction and supports containing TiO_2 [51–53] and very few including studies of electronic properties [54]. An electronic structure model was lately proposed suggesting that proximity of Fermi level of the support material and Fermi level of Pt to the redox potential of the reaction would enhance electrocatalytic activity [55]. Considering that the interaction Pt-support would shift the d-band center of Pt atoms modifying its electronic structure, an electronic transfer mechanism was proposed by Van Thi Thanh et al. [56].

In this work, to study the electronic properties of Pt on the different hybrid supports, *in situ* X-ray absorption spectroscopy (XAS) experiments were carried out around the Pt L_3 edge. Some absorption spectra are shown in Fig. 5a. The qualitative comparison of the absorption line of different spectra shows very subtle differences, as illustrated in Supplementary Fig. 2. The quantitative analysis of the XANES region of spectra was made using the method proposed by Shukla et al. [57], which consists in fitting the absorption spectrum to a theoretical curve that combines a Lorentzian curve to account for transitions to bound states with an arc tangent curve referred to the transitions to the continuum. The value of the integral of the Lorentzian curve can be used to assess the vacancy of the Pt 5d band (*i.e.,* higher values indicate that the Pt 5d band is more vacant and lower values evidence a more filled band). It was not possible to make that calculation for the catalyst supported on the C-WO_3 hybrid because of the overlapping of the W L_2 and the in Pt L_3 signals [58]. A plot of the integral of the Lorentzian curve for all the other catalysts studied in this work overlaid with the EOR current measured after 45 min polarization at 0.5 V (RHE) is depicted in Fig. 5b.

The correlation between the EOR activity and the Pt 5d band vacancy seems quite clear. At the same time, comparison of Pt supported on C-MOx hybrids and on Pt/C evidences that an enhancement of EOR current is observed if the hybrid support contributes to increase the Pt 5d band vacancy while metal-support interactions that result in a more filled band are detrimental to EOR activity. The electronic transfer mechanism proposed by Van Thi Thanh et al. [56] explains the correlation between electrocatalytic activity for EOR and the Pt 5d band vacancy depicted in Fig. 5b. As a whole, experimental results seem to evidence that metal-support interactions shift the Fermi level of Pt resulting in new electronic states (vacant or filled). Changes in electronic properties associated to varying amounts of oxidized species have been shown to influence the activity for the oxidation of alcohols also in acid solutions [59,60].

Seeking a better understanding of the differences in EOR activities revealed by electrochemistry and XAS results, further studies were conducted for the catalysts that showed the highest and lowest EOR activities (Pt/C–TiO_2 and Pt/C–CeO_2, respectively) and for the reference sample (Pt/C).

CO stripping experiments were performed in order to determine if the observed variations in EOR activity could be related to the removal of poisons upheld by oxygenated species provided by the transition metal oxides. For Pt/C–CeO_2 and Pt/C–TiO_2 catalysts, the CO stripping curves exhibit a current shoulder followed by two

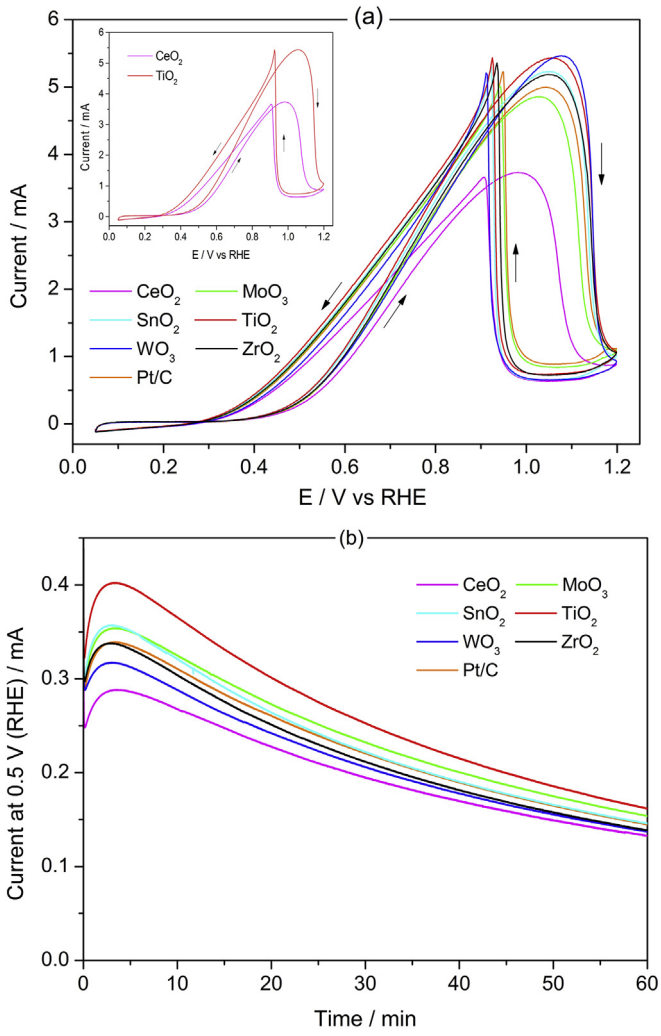

Fig. 4. (a) CV curves recorded in Ar-saturated 0.5 M ethanol + 0.1 M KOH solution at 50 mV s^{-1} and 900 rpm rotation for the Pt nanoparticles on different C-MOx hybrid supports. Inset: comparison of the curves for Pt supported on C–CeO_2 and C–TiO_2 hybrids. (b) CA curves of ethanol oxidation at 0.5 V. Curves for carbon-supported Pt nanoparticles are included for comparison. Electrode geometric area: 0.196 cm^2; Pt active area: 1.7 cm^2.

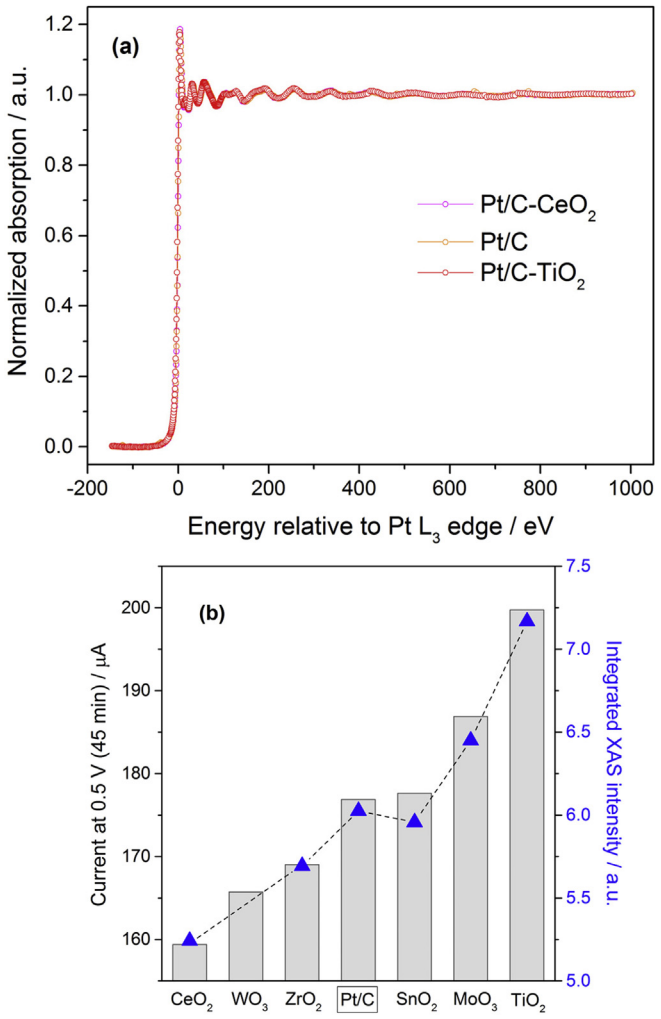

Fig. 5. (a) Comparison of X-ray absorption spectra of Pt/C–CeO_2, Pt/C and Pt/C–TiO_2, taken at 0.5 V. (b) Plot of the EOR current overlaid with the integrated XAS intensity of spectra taken at 0.5 V for the catalysts on hybrid supports containing different MOx transition metal oxides. For EOR currents: electrode geometric area: 0.196 cm^2; Pt active area: 1.7 cm^2.

well-defined current peaks with a slight difference in the potential at which the first current peak of CO oxidation appears, as illustrated in Supplementary Fig. 3. CO stripping curves like those observed in this work were reported in the literature for polycrystalline Pt electrodes [61–63]. The multiplicity of peaks was interpreted in terms of a single form of adsorbed CO being oxidized with the participation of PtOH of different energy [61], as associated to CO in bridge and linear forms [62] and, more recently, by suggesting that besides the CO adsorption energy, water and/or OH adsorption and their effects on CO mobility should be considered [63]. Differences in CO oxidation on catalysts containing transition metal oxides have been often interpreted as associated to oxygenated species supplied by the oxide [30,31], but considering the XAS results discussed above the slight difference in the position of the first current maximum could also arise from a variation of chemisorption energies of CO and/or OH on the Pt surface.

In situ FTIR spectroscopy measurements were performed aiming to analyze the effects of the hybrid supports on the distribution of reaction products. These experiments were carried out using a SCE reference electrode and all potentials are informed against it unless otherwise stated.

In situ MS-FTIR spectra of ethanol oxidation on Pt/C–TiO_2, Pt/C–CeO_2 and Pt/C catalysts, taken at potentials between −0.70 and 0.20 V vs SCE at 0.1 V intervals, are shown in Supplementary Fig. 4. The two upward IR bands at 1085 and 1045 cm^{-1} that are observed in all the spectra are characteristic of the C–O stretch of adsorbed ethanol and can be assigned to the consumption of ethanol due to its oxidation. Two downward bands at 1550 and 1415 cm^{-1} can be attributed to acetate ion (CH_3COO^-). In a general manner, ethanol oxidation in alkaline solution involves the following reactions:

$$CH_3CH_2OH + 5OH^- \rightarrow CH_3COO^- + 4H_2O + 4e \quad (2)$$

$$CH_3CH_2OH + 12OH^- \rightarrow 2CO_2 + 9H_2O + 12e \quad (3)$$

$$CO_2 + 2OH^- \rightarrow CO_3^{2-} + H_2O \quad (4)$$

The presence of CO_3^{2-} indicates that, to some extent, the complete oxidation of ethanol takes place. However, the band of CO_3^{2-} at 1390 cm^{-1} cannot be distinguished from the broad peak of CH_3COO^- at 1415 cm^{-1} as shown in Supplementary Fig. 4. On the

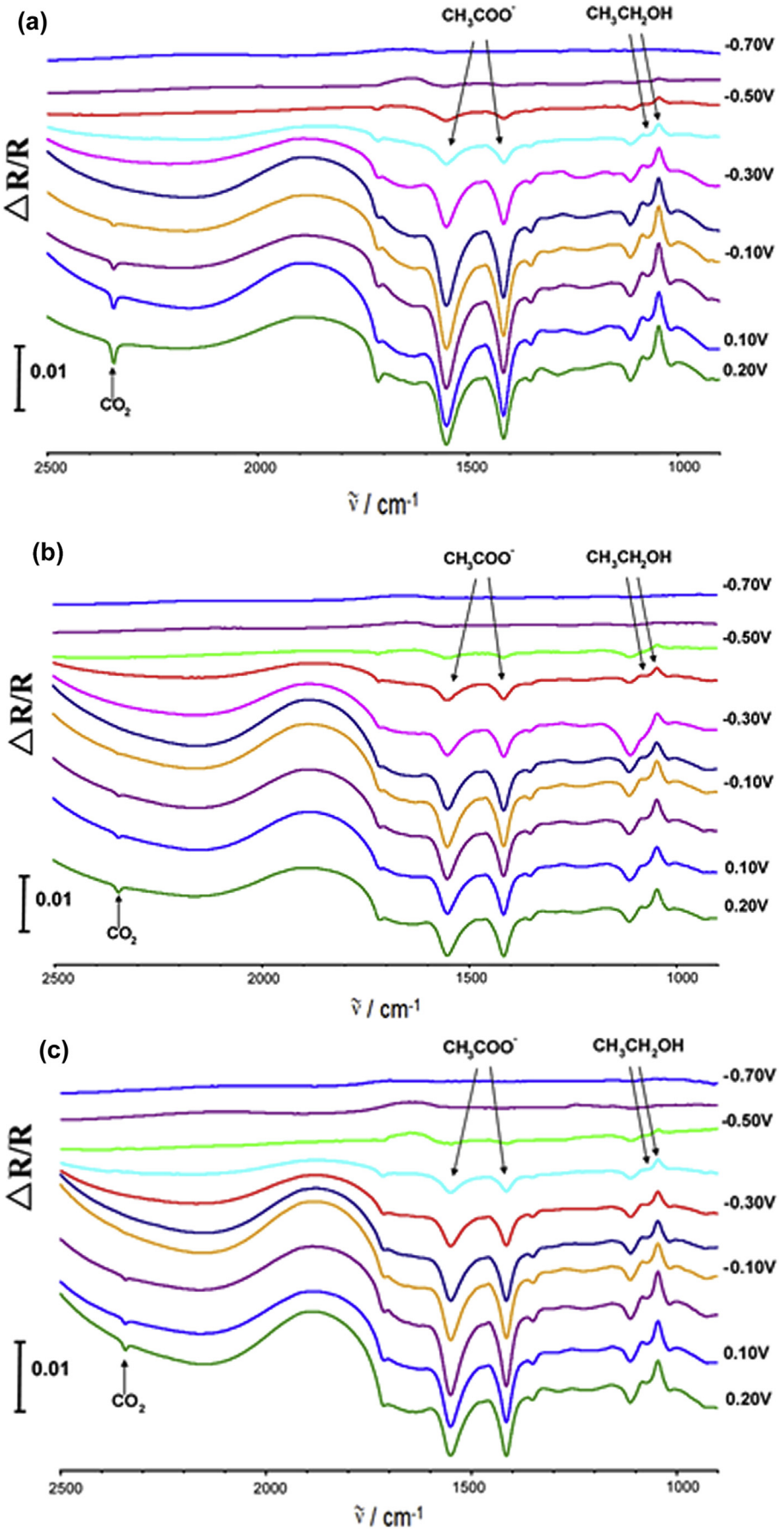

Fig. 6. In situ SPA-FTIR spectra of ethanol electro-oxidation on (a) Pt/C–TiO_2, (b) Pt/C and (c) Pt/C–CeO_2 catalysts at different potentials in 0.1 M NaOH + 0.5 M ethanol. E_S was varied from −0.70 to 0.20 V, E_R = −0.90 V, 400 scans, 8 cm^{-1}.

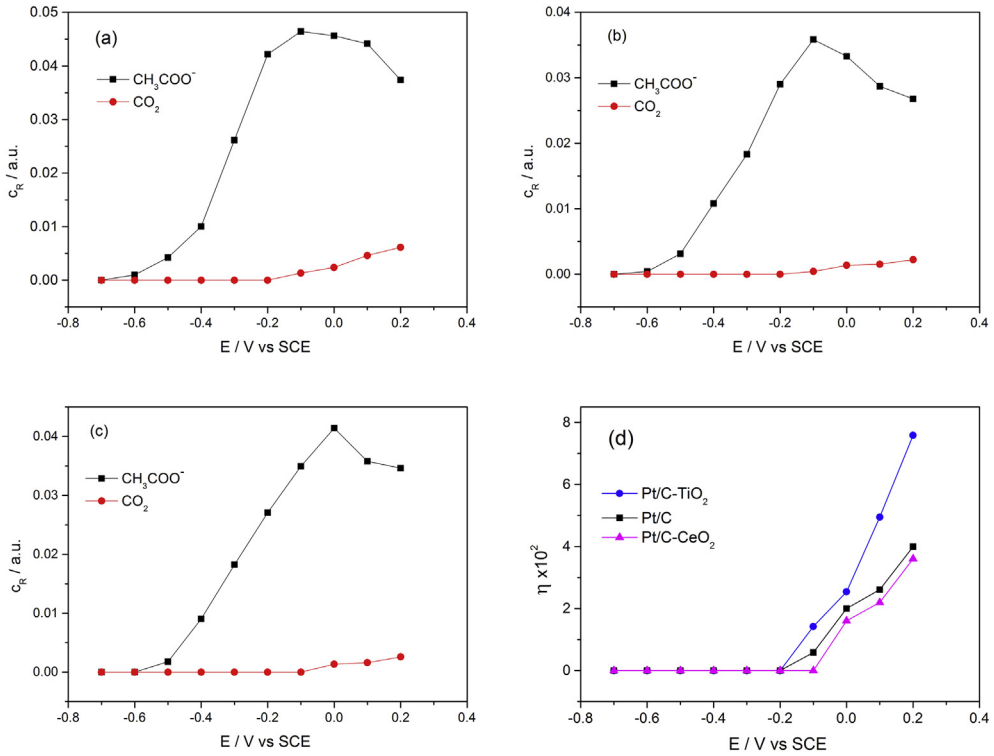

Fig. 7. Potential dependence of relative concentration (c_R) of CH_3COO^- and CO_2 generated from ethanol oxidation on (a) Pt/C–TiO_2, (b) Pt/C and (c) Pt/C–CeO_2 catalysts. (d) Potential dependence of the selectivity (η) for complete ethanol oxidation to CO_2.

other hand, the appearance of CO_2 at 2434 cm^{-1} suggests that at high potentials most of the NaOH in the thin-layer solution has been neutralized due to ethanol oxidation. The peak of CO_2 appears at $E > -0.10$ V for the catalysts Pt/C–TiO_2 and Pt/C (Supplementary Fig. 4a and 4b), while it is apparent only at $E > 0.0$ V for Pt/C–CeO_2 (Supplementary Fig. 4c).

To investigate further the ethanol oxidation ability of the three catalysts, series of *in situ* SPA-FTIR experiments were performed at different potentials for quantitative analysis of the products. Different from *in situ* MS-FTIR spectra, *in situ* SPA-FTIR spectrum was taken by collecting respectively only one single beam spectrum R(E_S) and one R(E_R) at E_S and E_R and, therefore, the accumulation of the products at different potentials can be ignored. Fig. 6 shows the series of *in situ* SPA-FTIR spectra of ethanol oxidation obtained at potentials varying from −0.70 to 0.20 V (vs SCE) at intervals of 0.10 V. We used the method previously proposed for *in situ* SPA-FTIR data [64], which consists in the subtraction of spectra to calculate the relative concentration of the products formed during the ethanol electro-oxidation [65]. In this method, we firstly collected IR transmission spectra of 0.02 M CH_3COONa, 0.02 M Na_2CO_3 and CO_2 saturated solution. Applying the subtracting operation to the *in situ* spectrum with the transmission spectra as subtrahend (that is, C = A−*k*B, where A is an *in situ* spectrum, B is the transmission spectrum, and *k* is a coefficient), we can evaluate the relative concentration (c_R) of each species, as shown in Supplementary Fig. 5. The peak at 1390 cm^{-1} is not apparent in spectrum C. That may be ascribed to the catalytic activity of the catalysts under potentials between −0.7 and 0.2 V (vs SCE) been very high, and, thus, consuming most of the NaOH in the thin-layer between the CaF_2 window and the electrode. That would make the concentration of OH^- too low for the formation of CO_3^{2-}.

The values of c_R for CH_3COO^- and CO_2 were obtained after subtracting from each spectrum the transmission spectrum of 0.02 M CH_3COONa and CO_2 respectively. Fig. 7a–c shows the potential dependence of the c_R of CH_3COO^- and CO_2 in the thin-layer solution during ethanol oxidation. The c_R of CH_3COO^- increases rapidly for potentials higher than −0.60 V (SCE) and then decreases slightly. The potential where the c_R of CH_3COO^- begins to decrease is somewhat different for the three catalysts (from −0.10 V for Pt/C–TiO_2 and Pt/C and from 0.0 V for Pt/C–CeO_2). In contrast, the c_R of CO_2 is rather low, indicating that complete oxidation of ethanol only takes place to a small extent. The c_R of CO_2 curve starts at E > −0.10 V for Pt/C–TiO_2 and Pt/C and at 0.0 V for Pt/C–CeO_2.

The ability to break C–C bond is a very important criterion for evaluating the efficiency of electrocatalysts for ethanol oxidation. Based on the relative concentrations obtained (Fig. 7a–c) we evaluate the selectivity for ethanol oxidation to CO_2 (η) as:

$$\eta = \frac{\frac{[CO_3^{2-}]+[CO_2]}{2}}{[CH_3COO^-] + \frac{[CO_3^{2-}]+[CO_2]}{2}} \quad (5)$$

The values of the concentration of CO_3^{2-} were negligible for all the catalysts under those potentials because, as shown in Supplementary Fig. 5, there is no obvious peak at 1390 cm^{-1} for the result spectrum after the subtracting operation. Fig. 7d illustrates the relationship between η and electrode potential. Clearly, the value of η is quite low for ethanol oxidation on the three catalysts. Therefore, the oxidation of ethanol on these materials is, as expected, quite incomplete and the main production is acetate.

Differences in activity of catalysts containing transition metal oxides have been often interpreted as associated to oxygenated species supplied by the oxide [30,31]. However, XAS experiments clearly evidence that the interactions between the Pt particles and the hybrid supports promote changes in the Pt 5d band vacancy, which affect the rate of the EOR as evidenced by data of Fig. 5. Overall, FTIR results show, as expected, that the main product of ethanol oxidation is acetate. It is also apparent that the extent of

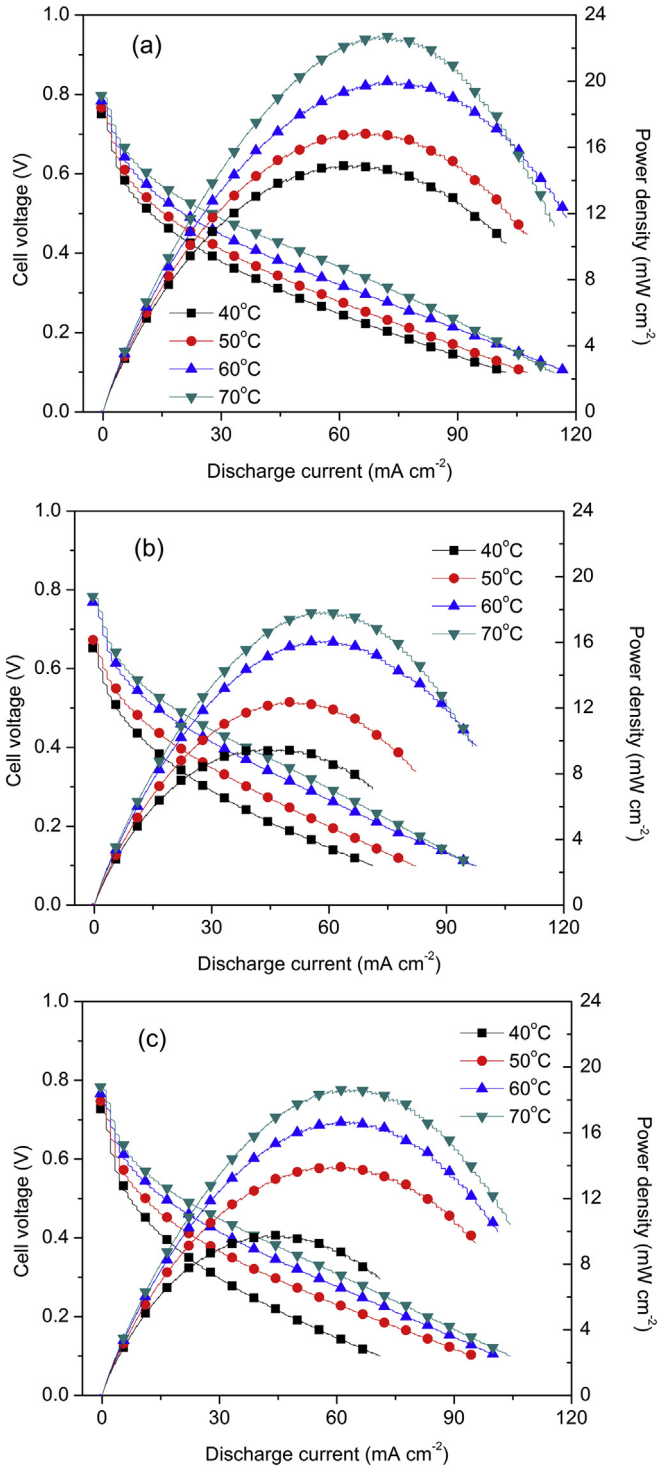

Fig. 8. Cell voltage and power density as a function of discharge current density at different temperatures. Anode catalysts: (a) Pt/C–TiO_2, (b) Pt/C–CeO_2 and (c) Pt/C. Feeding solution: 2 M ethanol +0.1 M KOH.

complete oxidation is rather small although there are differences in the amounts of CO_2 produced. In principle, the variation of electronic properties might have an effect on chemisorption energies and/or the strength of chemical bonds that have to break for the reaction to proceed. Ethanol adsorption is the first step of EOR, involving either C–H bond or O–H bond breaking that would produce, respectively, species adsorbed through the carbon atom or through the oxygen atom. This last possibility was, for instance, proposed by Iwasita and Pastor from studies of ethanol adsorption on polycrystalline Pt in acid solution [66]. More recently, Christensen et al. concluded that their FTIR results indicate that in alkaline solution ethanol oxidation on polycrystalline Pt lead to high coverages of adsorbed ethoxy even at low potentials [67]. Both cases are compatible with electronic properties having an effect on the EOR rate. Electronic properties could also affect the chemisorption energy of adsorbed OH species needed for the reaction to go on. Furthermore, the differences in the production of CO_2 revealed by the FTIR data are also compatible with a weakening of the C–C bond promoted by a larger electronic vacancy of the Pt d band. Unfortunately, it is not possible at this time to distinguish between all these possibilities and/or to rule out any of them. Nonetheless, data demonstrate quite clearly that metal-support interactions affect the electronic properties of the Pt particles, which in turn, influence the catalytic activity for EOR and the extent of ethanol oxidation to CO_2.

While experiments using conventional electrochemical techniques such as CV and CA provide essential data to unveil fundamental aspects of electrocatalytic processes, more often than not these measurements do not match fuel cell testing results. The Pt/C–TiO_2 and Pt/C–CeO_2 catalysts and the reference sample Pt/C were further tested in direct ethanol fuel cell using 2 M ethanol and varying KOH concentration at temperatures 70, 80 and 90 °C, respectively. Details for fuel cell assembly and test procedures were described in the experimental section. Fig. 8 shows a comparison of polarization curves and the corresponding power density curves measured at different temperatures in a single cell fed with 2 M ethanol +0.1 M KOH. As expected, the performance improves as the temperature increases. At all temperatures the discharge currents and power densities decrease in the sequence Pt/C–TiO_2 > Pt/C > Pt/C–CeO_2, *i.e.* in good agreement with the trend observed in electrochemical results (Fig. 4). Measurements carried out varying the amount of KOH in the fuel feeding solution revealed that increasing the KOH concentration from 0.1 to 0.2 M produced a slight improvement (about 5%) in the case of the Pt/C–TiO_2 anode and slight drops of performance for Pt/C and Pt/C–CeO_2. Further increase of the KOH concentration has a detrimental effect on the performance for all three catalysts tested, as illustrated in Supplementary Fig. 6 for the alkaline DEFC with Pt/C–TiO_2 anode. KOH concentration effects on alkaline DEFCs performance were studied by Li et al. [68] that found that for the ethanol concentrations that they used in their study, the performance in the region of high current density first increased and then dropped as KOH concentration was raised. Based on that, these authors proposed that in terms of fuel cell performance there is an optimum KOH concentration. Further analysis of these effects is beyond the scope of this work.

In summary, for all conditions used in this work the performance for EOR of the catalysts follows the same trend in CV and CA measurements, FTIR spectroscopy experiments and fuel cell testing, and is clearly influenced by the Pt 5d band vacancy.

4. Conclusions

The relevance of metal-support interactions on the EOR in alkaline solutions has been examined by carrying out experiments on catalysts consisting of identical Pt nanoparticles supported on C-MOx hybrids (MOx = TiO_2, ZrO_2, SnO_2, CeO_2, MoO_3 and WO_3). We found that metal-support interactions in these materials promote changes in the electronic properties that influence the EOR activity. EOR currents differ depending on the transition metal (CeO_2 < WO_3 < ZrO_2 < C ≈ SnO_2 < MoO_3 < TiO_2) and increase following the rise in the Pt 5d band vacancy. Additional studies

were carried out for the catalysts that produced the lowest and highest EOR currents (Pt/C–CeO_2 and Pt/C–TiO_2). *In situ* FTIR spectroscopy measurements showed that, as expected, the main product is acetate at the time that revealed differences in the selectivity for ethanol oxidation to CO_2. Although a definite interpretation is not possible at this time, it is quite clear that differences appear associated to the differences in Pt 5d band vacancy that would affect chemisorption energies and/or the strength of chemical bonds that have to be broken. Fuel cell testing showed performances in excellent agreement with the trends observed in electrochemical and spectroscopy experiments. Altogether, data show that favorable metal-support interactions could be a valuable tool to improve fuel cell performance or to decrease the anode Pt loading.

Acknowledgements

We acknowledge collaborative financial support as part of the International Union of Pure and Applied Chemistry (IUPAC) International Funding Call on “Novel Molecular and Supramolecular Theory and Synthesis Approaches for Sustainable Catalysis”. This work was funded by Fundação de Amparo à Pesquisa do Estado de São Paulo (FAPESP), Brazil (2013/50206-4; 2014/12255-6), National Natural Science Foundation of China (NSFC), China (21361140374), and National Science Foundation (NSF), United States of America (Contract 1402422). Thanks are also due to the Brazilian Synchrotron Light Laboratory (LNLS) for assisting XAS experiments and to the Brazilian Nanotechnology National Laboratory (LNNano) for XPS measurements. DRMG thanks FAPESP for the fellowship granted (2013/01822-4).

Appendix A. Supplementary data

Supplementary data related to this article can be found at http://dx.doi.org/10.1016/j.jpowsour.2016.02.011.

References

[1] W. Vielstich, Ideal and effective efficiencies of cell reactions and comparison to carnot cycles, in: W. Vielstich, H.A. Gasteiger, A. Lamm (Eds.), Handbook of Fuel Cells: Fundamentals, Technology and Applications, John Wiley, New York, 2003, pp. 26–30.
[2] J. Baeyens, Q. Kang, L. Appels, R. Dewil, Y.Q. Lv, T.W. Tan, Prog. Energy Combust. Sci. 47 (2015) 60–88.
[3] S.P.S. Badwal, S. Giddey, A. Kulkarni, J. Goel, S. Basu, Appl. Energy 145 (2015) 80–103.
[4] A. Brouzgou, A. Podias, P. Tsiakaras, J. Appl. Electrochem. 43 (2013) 119–136.
[5] C. Lamy, S. Rousseau, E.M. Belgsir, C. Coutanceau, J.M. Leger, Electrochim. Acta 49 (2004) 3901–3908.
[6] F. Vigier, S. Rousseau, C. Coutanceau, J.-M. Leger, C. Lamy, Top. Catal. 40 (2006) 111–121.
[7] A. Brouzgou, S.Q. Song, P. Tsiakaras, Appl. Catal. B Environ. 127 (2012) 371–388.
[8] M.R. Tarasevich, O.V. Korchagin, A.V. Kuzov, Russ. Chem. Rev. 82 (2013) 1047–1065.
[9] L. Rao, Y. Jiang, B. Zhang, L. You, Z. Li, S. Sun, Prog. Chem. 26 (2014) 727–736.
[10] F. Colmati, G. Tremiliosi-Filho, E.R. Gonzalez, A. Berna, E. Herrero, J.M. Feliu, Phys. Chem. Chem. Phys. 11 (2009) 9114–9123.
[11] F. Colmati, G. Tremiliosi-Filho, E.R. Gonzalez, A. Berna, E. Herrero, J.M. Feliu, Faraday Discuss. 140 (2008) 379–397.
[12] Y.-Y. Li, L. Rao, Y.-X. Jiang, Z.-L. Liu, C.-L. He, B.-W. Zhang, S.-G. Sun, Chem. J. Chin. Univ. Chin. 34 (2013) 408–413.
[13] G.A. Camara, T. Iwasita, J. Electroanal. Chem. 578 (2005) 315–321.
[14] H. Wang, Z. Jusys, R.J. Behm, J. Phys. Chem. B 108 (2004) 19413–19424.
[15] Q. Wang, G.Q. Sun, L.H. Jiang, Q. Xin, S.G. Sun, Y.X. Jiang, S.P. Chen, Z. Jusys, R.J. Behm, Phys. Chem. Chem. Phys. 9 (2007) 2686–2696.
[16] M. Heinen, Z. Jusys, R.J. Behm, Prot. Exch. Membr. Fuel Cells 9 (25) (2009) 259–269.
[17] J.M. Perez, B. Beden, F. Hahn, A. Aldaz, C. Lamy, J. Electroanal. Chem. 262 (1989) 251–261.
[18] E. Antolini, J. Power Sources 170 (2007) 1–12.
[19] P.K. Shen, A.C.C. Tseung, J. Electrochem. Soc. 141 (1994) 3082–3090.
[20] A.K. Shukla, M.K. Ravikumar, A.S. Arico, G. Candiano, V. Antonucci, N. Giordano, A. Hamnett, J. Appl. Electrochem. 25 (1995) 528–532.
[21] H. Xu, X. Hou, Int. J. Hydrogen Energy 32 (2007) 4397–4401.
[22] C.W. Xu, P.K. Shen, J. Power Sources 142 (2005) 27–29.
[23] C.W. Xu, R. Zeng, P.K. Shen, Z.D. Wei, Electrochim. Acta 51 (2005) 1031–1035.
[24] C.L. Campos, C. Roldan, M. Aponte, Y. Ishikawa, C.R. Cabrera, J. Electroanal. Chem. 581 (2005) 206–215.
[25] Y.X. Bai, J.J. Wu, J.Y. Xi, J.S. Wang, W.T. Zhu, L.Q. Chen, X.P. Qiu, Electrochem. Commun. 7 (2005) 1087–1090.
[26] L. Jiang, L. Colmenares, Z. Jusys, G.Q. Sun, R.J. Behm, Electrochim. Acta 53 (2007) 377–389.
[27] J. Mann, N. Yao, A.B. Bocarsly, Langmuir 22 (2006) 10432–10436.
[28] H.M. Villullas, F.I. Mattos-Costa, L.O.S. Bulhoes, J. Phys. Chem. B 108 (2004) 12898–12903.
[29] H.M. Villullas, F.I. Mattos-Costa, P.A.P. Nascente, L.O.S. Bulhoes, Chem. Mater. 18 (2006) 5563–5570.
[30] P.J. Kulesza, I.S. Pieta, I.A. Rutkowska, A. Wadas, D. Marks, K. Klak, L. Stobinski, J.A. Cox, Electrochim. Acta 110 (2013) 474–483.
[31] Z. Zhang, J. Liu, J. Gu, L. Su, L. Cheng, Energy Environ. Sci. 7 (2014) 2535–2558.
[32] G. Couture, A. Alaaeddine, F. Boschet, B. Ameduri, Prog. Polym. Sci. 36 (2011) 1521–1557.
[33] G. Merle, M. Wessling, K. Nijmeijer, J. Membr. Sci. 377 (2011) 1–35.
[34] E. Antolini, E.R. Gonzalez, J. Power Sources 195 (2010) 3431–3450.
[35] L. Ma, D. Chu, R.R. Chen, Int. J. Hydrogen Energy 37 (2012) 11185–11194.
[36] L. Jiang, A. Hsu, D. Chu, R. Chen, Int. J. Hydrogen Energy 35 (2010) 365–372.
[37] S.H. Sun, C.B. Murray, D. Weller, L. Folks, A. Moser, Science 287 (2000) 1989–1992.
[38] E.I. Santiago, L.C. Varanda, H.M. Villullas, J. Phys. Chem. C 111 (2007) 3146–3151.
[39] A.L.N. Pinheiro, A. Oliveira-Neto, E.C. de Souza, J. Perez, V.A. Paganin, E.A. Ticianelli, E.R. Gonzalez, J. New Mater. Electrochem. Syst. 6 (2003) 1–8.
[40] J. McBreen, W.E. Ogrady, K.I. Pandya, R.W. Hoffman, D.E. Sayers, Langmuir 3 (1987) 428–433.
[41] L. Ma, H. He, A. Hsu, R. Chen, J. Power Sources 241 (2013) 696–702.
[42] W.F. Lin, S.G. Sun, Electrochim. Acta 41 (1996) 803–809.
[43] D.S. Corrigan, L.W.H. Leung, M.J. Weaver, Anal. Chem. 59 (1987) 2252–2256.
[44] J.F. Moulder, J. Chastain, R.C. King, Handbook of X-ray Photoelectron Spectroscopy: A Reference Book of Standard Spectra for Identification and Interpretation of XPS Data, Perkin-Elmer, Eden Prairie, MN, 1992.
[45] F. Sen, G. Gokagac, J. Phys. Chem. C 111 (2007) 5715–5720.
[46] S.J. Tauster, S.C. Fung, R.L. Garten, J. Am. Chem. Soc. 100 (1978) 170–175.
[47] J.A. Horsley, J. Am. Chem. Soc. 101 (1979) 2870–2874.
[48] B.H. Chen, J.M. White, J. Phys. Chem. 86 (1982) 3534–3541.
[49] M.G. Sanchez, J.L. Gazquez, J. Catal. 104 (1987) 120–135.
[50] S.J. Tauster, S.C. Fung, J. Catal. 55 (1978) 29–35.
[51] L. Xiong, A. Manthiram, Electrochim. Acta 49 (2004) 4163–4170.
[52] W. Vogel, L. Timperman, N. Alonso-Vante, Appl. Catal. A General 377 (2010) 167–173.
[53] A. Lewera, L. Timperman, A. Roguska, N. Alonso-Vante, J. Phys. Chem. C 115 (2011) 20153–20159.
[54] S.J. Yoo, T.-Y. Jeon, K.-S. Lee, K.-W. Park, Y.-E. Sung, Chem. Commun. 46 (2010) 794–796.
[55] F. Shi, L.R. Baker, A. Hervier, G.A. Somorjai, K. Komvopoulos, Nano Lett. 13 (2013) 4469–4474.
[56] H. Van Thi Thanh, C.-J. Pan, J. Rick, W.-N. Su, B.-J. Hwang, J. Am. Chem. Soc. 133 (2011) 11716–11724.
[57] A.K. Shukla, R.K. Raman, N.A. Choudhury, K.R. Priolkar, P.R. Sarode, S. Emura, R. Kumashiro, J. Electroanal. Chem. 563 (2004) 181–190.
[58] L.G.S. Pereira, V.A. Paganin, E.A. Ticianelli, Electrochim. Acta 54 (2009) 1992–1998.
[59] D.R.M. Godoi, J. Perez, H.M. Villullas, J. Power Sources 195 (2010) 3394–3401.
[60] D.R.M. Godoi, H.M. Villullas, Langmuir 28 (2012) 1064–1067.
[61] E. Santos, M.C. Giordano, J. Electroanal. Chem. 172 (1984) 201–210.
[62] H. Kita, K. Shimazu, K. Kunimatsu, Troanal. Chem. 241 (1988) 163–179.
[63] H. Wang, H.D. Abruna, J. Phys. Chem. Lett. 6 (2015) 1899–1906.
[64] Z.-Y. Zhou, D.-J. Chen, H. Li, Q. Wang, S.-G. Sun, J. Phys. Chem. C 112 (2008) 19012–19017.
[65] Z.-Y. Zhou, Q. Wang, J.-L. Lin, N. Tian, S.-G. Sun, Electrochim. Acta 55 (2010) 7995–7999.
[66] T. Iwasita, E. Pastor, Electrochim. Acta 39 (1994) 531–537.
[67] P.A. Christensen, S.W.M. Jones, A. Hamnett, J. Phys. Chem. C 116 (2012) 24681–24689.
[68] Y.S. Li, T.S. Zhao, Z.X. Liang, J. Power Sources 187 (2009) 387–392.